Instrumentation-related uncertainty of reflectance and transmittance measurements with a two-channel spectrophotometer

Christian Peest, Carsten Schinke, Rolf Brendel, Jan Schmidt, and Karsten Bothe

Citation: Review of Scientific Instruments **88**, 015105 (2017);
View online: https://doi.org/10.1063/1.4973633
View Table of Contents: http://aip.scitation.org/toc/rsi/88/1
Published by the American Institute of Physics

Articles you may be interested in

Photon counting phosphorescence lifetime imaging with TimepixCam
Review of Scientific Instruments **88**, 013104 (2017); 10.1063/1.4973717

Note: A high-performance, low-cost laser shutter using a piezoelectric cantilever actuator
Review of Scientific Instruments **88**, 016102 (2017); 10.1063/1.4973774

Continuous time of flight measurements in a Lissajous configuration
Review of Scientific Instruments **88**, 013301 (2017); 10.1063/1.4971305

Thermoelectric characterization of flexible micro-thermoelectric generators
Review of Scientific Instruments **88**, 015103 (2017); 10.1063/1.4973417

Simple quadratic magneto-optic Kerr effect measurement system using permanent magnets
Review of Scientific Instruments **88**, 013901 (2017); 10.1063/1.4973419

Simultaneous measurement of in-plane and through-plane thermal conductivity using beam-offset frequency domain thermoreflectance
Review of Scientific Instruments **88**, 014902 (2017); 10.1063/1.4973297

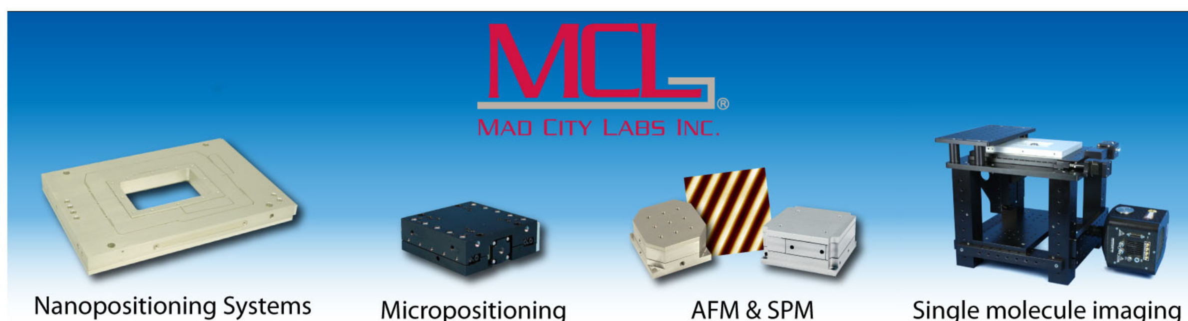

CrossMark

Instrumentation-related uncertainty of reflectance and transmittance measurements with a two-channel spectrophotometer

Christian Peest,[1,a)] Carsten Schinke,[1,2] Rolf Brendel,[1,2] Jan Schmidt,[1,2] and Karsten Bothe[1]
[1]*Institute for Solar Energy Research Hamelin (ISFH), Am Ohrberg 1, 31860 Emmerthal, Germany*
[2]*Leibniz University of Hanover (LUH), Institute for Solid State Physics, Appelstr. 2, 30167 Hanover, Germany*

(Received 29 June 2016; accepted 22 December 2016; published online 12 January 2017)

Spectrophotometers are operated in numerous fields of science and industry for a variety of applications. In order to provide confidence for the measured data, analyzing the associated uncertainty is valuable. However, the uncertainty of the measurement results is often unknown or reduced to sample-related contributions. In this paper, we describe our approach for the systematic determination of the measurement uncertainty of the commercially available two-channel spectrophotometer Agilent Cary 5000 in accordance with the *Guide to the expression of uncertainty in measurements*. We focus on the instrumentation-related uncertainty contributions rather than the specific application and thus outline a general procedure which can be adapted for other instruments. Moreover, we discover a systematic signal deviation due to the inertia of the measurement amplifier and develop and apply a correction procedure. Thereby we increase the usable dynamic range of the instrument by more than one order of magnitude. We present methods for the quantification of the uncertainty contributions and combine them into an uncertainty budget for the device. *Published by AIP Publishing.* [http://dx.doi.org/10.1063/1.4973633]

I. INTRODUCTION

Spectrophotometry is a widely used measurement technique in many fields of natural and life science.[1–3] Usually, it is believed to be a very accurate and reliable measurement technique. Thus, most published uncertainty considerations focus on the impact of sample-related contributions to the uncertainty budget, whereas the impact of the instrumentation is believed to be of minor significance and is therefore not considered.[4,5] However, in order to obtain accurate and reliable data, a comprehensive analysis not only of the sample under test but also of the spectrophotometer itself as well as the measurement procedure is required. The ASTM standard "Estimating Uncertainty of Test Results Derived from Spectrophotometry,"[6] subdivided into instrument, operator, and uniformity uncertainty contributions, can be regarded as a guideline for such an analysis. Some of the mentioned contributions are discussed in Ref. 7.

This paper focuses on the experimental determination of the uncertainty contributions caused by the instrumentation. We consider a widely used commercially available spectrophotometer, the Agilent Cary 5000 UV-VIS-NIR. This device is used world wide for research and development, for quality assurance as well as for calibration measurements. We present methods for the quantitative estimation of the instrument-related uncertainty contributions, taking into account that such a commercially available system provides only limited access to the parameters required for a comprehensive uncertainty analysis. In accordance with the *Guide to the expression of uncertainty in measurement* (GUM),[8] the different contributions are combined into an uncertainty budget. For specific applications, sample and measurement procedure related contributions have to be added to this budget. However, the number of applications is numerous and can thus not be treated in a general way. As an example, we show an uncertainty analysis for reflectance and transmission measurements on planar silicon wafers in Section V, which also takes sample-related contributions to the uncertainty budget into account.

II. METHODOLOGY

The analysis presented in this work is based on an extensive characterization of an Agilent Cary 5000 spectrophotometer. We apply the methodology specified in the GUM,[8] which is an internationally accepted standard procedure for the determination of the uncertainty of an *output quantity* or *measurand* y which is not measured directly but calculated from other quantities (*input quantities*).[8] The GUM presumes that all known and relevant effects leading to systematic deviations of the measurement result (often called *error* or *systematic error*) are avoided or corrected. Unknown errors, which arise from incomplete knowledge about the measurement object and the measurement procedure and obviously cannot be corrected, are included into the uncertainty budget which is then evaluated using the GUM procedure. Figure 1 sketches the difference of systematic deviations, which lead to a different *expectation value* for the measurement result, and uncertainties, which lead to a *distribution* of the measurement result. The GUM distinguishes between two ways of determining uncertainty contributions (A and B). Type A denotes contributions which are determined from repeated observations of a quantity. Type B denotes all other contributions, which are not determined from repeated measurements but follow, e.g., from a physical model, a calibration certificate or

[a)]Now with Sterrenkundig Observatorium, Universiteit Gent, Krijgslaan 281 S9, 9000 Gent, Belgium; Electronic mail: christian.peest@ugent.be

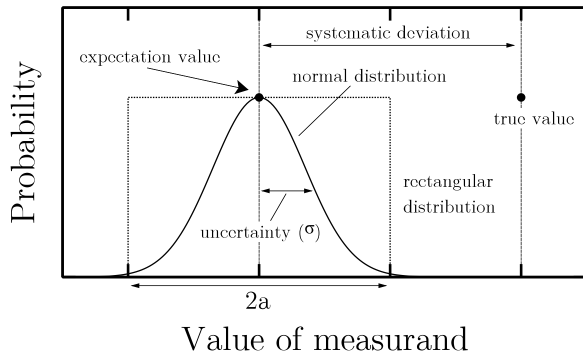

FIG. 1. Visualization of the terms *systematic deviation* and *uncertainty*.

scientific experience. The nomenclature does not refer to the treatment of the uncertainty contributions, which is equal for both types. Note that type A and B must not be confused with the familiar terms *systematic error* and *random error*, which describe the nature of the error. Each determination type (A or B) can in principle be used to determine the uncertainty due to errors of both types.

The core part of an uncertainty analysis in accordance with the GUM is the *process equation* f, which defines the functional relationship between the measurand y and input quantities $x_1, x_2, \ldots, x_N$,

$$y = f(x_1, x_2, \ldots, x_N). \tag{1}$$

The *combined standard uncertainty* $u_c^2(y)$ of the measurand y is then given by

$$u_c^2(y) = \sum_{i=1}^{N}\sum_{j=1}^{N} \frac{\partial f}{\partial x_i}\frac{\partial f}{\partial x_j} u\left(x_i, x_j\right). \tag{2}$$

If the x_i are uncorrelated, which means that the values of the x_i are not affected by the values of the other $x_{j\neq i}$, this simplifies to

$$u_c^2(y) = \sum_{i=1}^{N} \left(\frac{\partial f}{\partial x_i}\right)^2 u^2(x_i) = \sum_{i=1}^{N} c_i^2 u_i^2, \tag{3}$$

with the *sensitivity coefficients* $c_i = {}^{\partial f}/_{\partial x_i}$ and the uncertainty of the input quantities $u(x_i) \equiv u_{\mathrm{i}}$. The case of uncorrelated input quantities is assumed throughout this paper due to the physical origin of the uncertainty contributions or the quantification method (see comments in Section IV).

The formulation of the complete process equation is a critical part of the evaluation of measurement uncertainty, as it must include all relevant effects that could lead to systematic deviations of the measurement result, as mentioned above. Alternatively, corrections can directly be applied to the input quantities, and a simpler process equation (without correction terms) can be used. It is obvious that both approaches are equivalent. Furthermore, the uncertainty distributions of the input quantities need to be determined. Recurrent distributions are the normal and the rectangular distribution (see Fig. 1). The first describes values randomly scattered around the mean value, whereas the latter is used when the exact distribution is unknown but the upper and lower boundaries are known, in between which the true value lies.

For all mentioned distributions, the best estimate of the true value is the arithmetic mean of a number N of repeated measurements. For the normal distribution (ND), the uncertainty of the estimated value is given by

$$u_{\mathrm{ND}}^2 = \frac{\sigma^2}{\sqrt{N-1}}, \tag{4}$$

with the variance σ^2 of the arithmetic mean. Note that in principle, a limited number of measurements is described by the Student's t-distribution rather than the normal distribution. For a large number of measurements, however, the t-distribution approaches the normal distribution. (see Sec. IV A and GUM Annex C). The rectangular distribution represents a uniform probability density (UD) of width $2a$. The associated uncertainty is

$$u_{\mathrm{UD}}^2 = \frac{a^2}{3}. \tag{5}$$

The true value lies within the interval $\pm u_c$ around the measured value with a probability of approximately 68%. The expanded uncertainty U for the coverage factor k is defined as

$$U = k \cdot u_c. \tag{6}$$

In this paper, all given expanded uncertainties refer to a coverage factor of $k = 2$, i.e., they encompass the true value with a probability of about 95%.

III. MEASUREMENT SETUP

The spectrophotometer under test is an *Agilent Cary 5000* two-channel-spectrophotometer equipped with the *Diffuse Reflectance Accessory*. A sketch of this instrument is shown in Figure 2. Monochromatic light is generated using either a deuterium arc or a tungsten halogen light source in combination with a grating double monochromator. By a rotating mirror, the light is guided into different directions in a repeating sequence of three steps with a frequency of 33 Hz. During the first step, the light is directed through the monitor channel into the integrating sphere, whereas during the second step, it is focused on the sample. During the third step, the light is blocked.

The light level in the integrating sphere is measured with either a lead sulfide detector (PbS) or a photomultiplier (PM). During the first step, the *monitor signal* S_{Mon} is measured in order to correct for variations of the source brightness over time. Moreover, this measurement is used to adjust the amplification

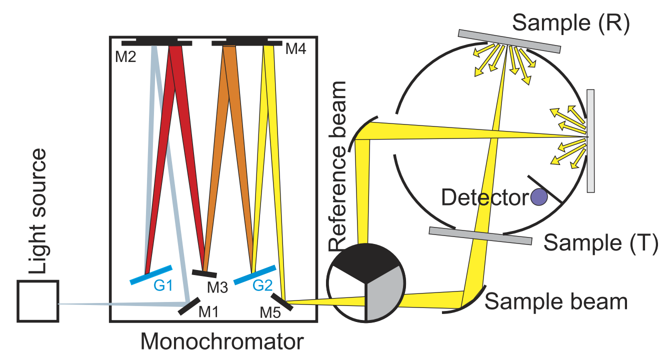

FIG. 2. Schematic setup of the Agilent Cary 5000 UV-VIS-NIR. Mirrors are labeled $M1$ to $M5$, gratings are labeled $G1$ and $G2$.

factor g_{amp} of the measurement amplifier. During the second step, the *sample signal* S_{Sam} is measured. In the third step, the *baseline signal* S_{Bas} is measured, which contains detector and electronic offsets and stray light.

In order to determine the reflectance of a sample, three measurements are combined: One measurement with a calibrated standard on the reflection port (R_N), one with the sample in the same position (R_S), and a baseline measurement with the reflection port open to a darkened room (R_B). R_B determines the amount of light that is reflected back into the integrating sphere at the edge of the reflectance port, and R_N is used to normalize the measurement of the sample, so that the reflectivity of the sample can be calculated with the tabulated reflectivity R_{Std} of the standard,

$$R = \frac{R_S - R_B}{R_N - R_B} R_{Std}. \quad (7)$$

For transmittance measurements, this procedure is simplified. The baseline measurement, a measurement with a beam trap, is omitted. This is possible due to an internal baseline correction (see Eq. (9)). For the measurements considered in this paper (wavelength range 250 nm–1450 nm), the absorption of light in air is negligible; therefore an empty transmission port replaces the measurement of a calibrated standard. Hence, only two measurements are required: one measurement with the sample in the transmission port of the integrating sphere (T_S) and one with an empty transmission port (T_N). The transmittance of the sample is then given by

$$T = \frac{T_S}{T_N}. \quad (8)$$

Each of the input quantities $S \in \{T_N, T_S, R_B, R_N, R_S\}$ is given by

$$S = \frac{S_{Sam} - S_{Bas}}{S_{Mon} - S_{Bas}}, \quad (9)$$

where S_{Mon}, S_{Sam}, and S_{Bas} denote the detector signal during the mentioned three steps (illumination of monitor channel, illumination of sample channel, baseline measurement), respectively. These quantities are not accessible to the operator and the calculation of S is carried out internally by the instrument.

A. Settings for data acquisition

According to the manufacturer default settings of the Agilent Cary 5000, the PM detector is used for wavelengths below 800 nm and the PbS detector for wavelengths above 800 nm. Moreover, a grating change occurs at 800 nm. For measurements with the PM detector, the spectral bandwidth $\Delta\lambda$ of the monochromator is set to a constant value and the amplification factor of the measurement preamplifier is varied in order to obtain an optimal modulation of the analog-to-digital converter (ADC). For the PbS detector, optimal modulation of the ADC is achieved by keeping the amplification factor constant and varying the spectral bandwidth between 1 nm and 20 nm during the scan. Figure 3 exemplary shows the result of a reflectance measurement of a silicon solar cell using the manufacturer default settings (red curve). The top graph shows the standard deviation σ_{25} of 25 repeated measurements. Obviously, the setting for the grating change wavelength leads to increased random noise at wavelengths above 800 nm. Moreover, in the view of data correction and uncertainty analysis, a variable spectral bandwidth is difficult to handle since $\Delta\lambda$ is not recorded as a function of wavelength by the operation software. On the other hand, variations of noise related to a varying amplification factor are easily quantified by repeated measurements. In order to circumvent the mentioned problems and to achieve a decreased random noise above 800 nm, we separate the grating change from the detector change, change the grating already at 700 nm, and extend the usage of the PM detector to 960 nm. Furthermore, we set a constant spectral bandwidth of 8 nm for the PbS detector. The resulting data using these settings are visualized by the dashed blue curves in Fig. 3. With these settings, we do not observe increased noise above 800 nm. The top graph shows that for the chosen sample, the noise of the PbS detector decreases from 800 nm to 1000 nm (red curve), whereas the noise of the PM detector is significantly lower at 800 nm but increases towards longer wavelengths. Both noise levels are approximately equal at 960 nm. Hence, this wavelength is a reasonable choice for the detector change. The slightly increased noise above 1000 nm when using our settings is a consequence of the fixed spectral bandwidth of 8 nm. When applying the manufacturer default settings, a larger spectral bandwidth is used in this wavelength range and leads to a larger detector signal (which means less noise). Note that the optimum wavelength for the detector change depends on the measurement signal and thus on the sample. It can easily be determined by recording the standard deviation of repeated measurements as a function of the wavelength with both detectors. Also note that the choice of $\Delta\lambda$ = 8 nm is a trade-off between increased measurement noise and an increasing uncertainty contribution related to the spectral bandwidth and results from our uncertainty analysis. Details are given in Section IV.

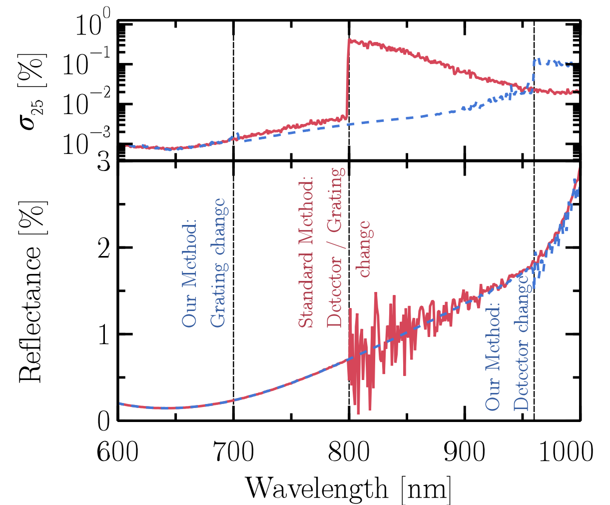

FIG. 3. Adjustment of the device settings. Acquisition time for each wavelength: 2.5 s. Red: Measurement with manufacturer default settings, detector and grating changeover at 800 nm, PbS with variable spectral bandwidth. Blue: our configuration, grating change at 700 nm and detector at 960 nm; PbS with a fixed spectral bandwidth $\Delta\lambda$ = 8 nm. The bottom graph shows the measured reflectance and the top graph the standard deviation σ_{25} of 25 repeated measurements.

B. Systematic deviation caused by the PbS detector

The calculation of the measurand (R or T) using Eqs. (7)–(9) requires the correct determination of the baseline signal S_{Bas}. Since the light level on the detector varies over time with a frequency of 33 Hz due to the rotating mirror (see Section III), it is necessary that S_{Bas} is time-independent. This condition is tested by setting up the instrument for transmittance measurements and placing a beam trap at the sample port. According to Eq. (9), the resulting signal S_0,

$$S_0 = T_{trap}/T_N \ , \tag{10}$$

should then be zero due to $S_{Sam} = S_{Bas}$. Operating the instrument in reverse mode, i.e., toggling sample and monitor channel, and placing the beam trap at the monitor port, should yield the same result. For the PM, we find $S_0 = 0$ in both normal and reverse modes. For the PbS detector, however, we find a systematic deviation from the expectation value of zero, which is mostly independent of the wavelength. The data are visualized in Fig. 4. Operating the instrument in the reverse mode leads to a comparable deviation of opposite sign. This points towards a time dependence of the baseline signal S_{Bas} as the source of the deviation rather than stray light, which would be expected to result in a positive deviation in both cases. Moreover, the absolute value of the deviation is found to depend on the amplification factor g_{amp} of the measurement amplifier (see Fig. 6), which shows that the amplifier is likely the source of the deviation.

Figure 5 depicts a possible model for the amplifier signal as a function of time. The light level on the detector is assumed to change instantly with a frequency of $1/\tau$. The output signal of an ideal amplifier, visualized by the dotted line, follows the changes immediately. Signal sampling with a constant frequency at the times t_{Mon}, t_{Sam}, and t_{Bas} yields the correct signals S_{Mon}, S_{Sam}, and S_{Bas}. The output signal of the real amplifier (solid line) cannot follow the changes immediately. In Fig. 5, an exponential decay is assumed. In this case, the signals $S'_{Mon} < S_{Mon}$, $S'_{Sam} < S_{Sam}$, and $S'_{Bas} > S_{Bas}$ would be measured. For the test measurement with the beam trap, $S_{Sam} = S_{Bas}$ but $S'_{Sam} \neq S'_{Bas}$ and thus $S' \neq 0$ according to Eq. (9). This conclusion is also correct if we assume another decay function, e.g., a linear decay of the signal, and/or an integration of the signal over time instead of sampling the signal at distinct times.

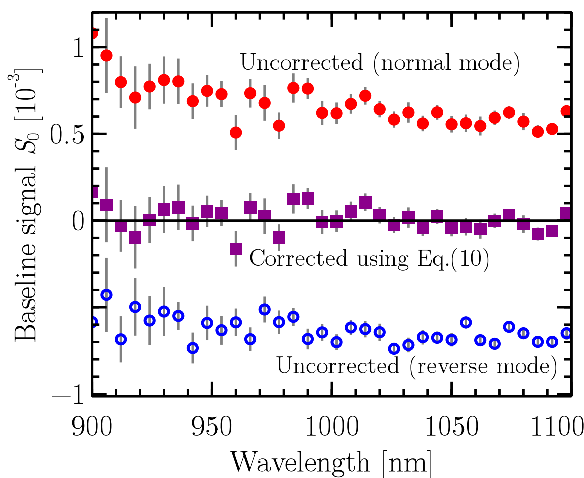

FIG. 4. Baseline signal S_0 of the PbS-detector as defined in Eq. (10). S_0 is measured by placing a beam trap at the sample port and performing a transmittance measurement. A slit width of 8 nm is used. The error bars represent the uncertainty of the mean, determined from 25 measurements. The amplification factor g_{amp} is 25 at 900 nm and 5 at 1100 nm.

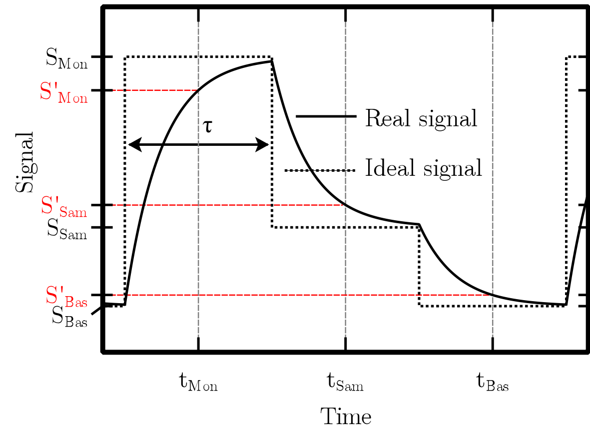

FIG. 5. Possible model for the amplifier output signal as a function of time. The dotted line represents the ideal signal, which follows the changes of the light level immediately. The real signal (solid line) cannot follow the changes immediately.

One option to prevent the systematic deviation of S would be a reduction of the mirror frequency (i.e., an enlargement of the time interval τ) in order to allow the signal to reach its saturation value before sampling. However, this is technically not possible due to a limited access to the device parameters in the operation software. Therefore, we apply a mathematical data correction based on a physical model of the measurement process. The model leads to the correction formula

$$S = \frac{S' - S_0}{1 - S_0 + S' S_0}, \tag{11}$$

for the measured and corrected signals $S' \in \{R', T'\}$ and $S \in \{R, T\}$, respectively, using the baseline signal S_0 resulting from the beam trap measurement. Details on the model and the derivation are given in the Appendix. The value S_0 can be determined in two ways. One is to measure it separately for each transmission measurement, similar to the baseline R_B in measurements of reflectance. The other is based on the observed relationship between S_0 and g_{amp} which is shown in Figure 6. This curve is acquired by averaging the measured value S_0 over many measurements. For our instrument, the relation is

$$S_0 = 0.0525\% + 0.001\,57\% \cdot g_{amp}. \tag{12}$$

The advantage of using this relation is the reduction of measurement noise, as during the sample analysis the signal is usually not averaged over as many repetitions, for practical reasons. Note that the operation software of the Cary is not capable of logging g_{amp} (denoted as *Energy Level* in the software). We therefore use an additional, self-made software tool for this task in parallel to the operation software.

The violet data points in Figure 4 show the result of the correction for the beam trap measurement in the normal mode (red circles). The corrected values are found to scatter around their expectation value of zero. Potential residual uncertainties

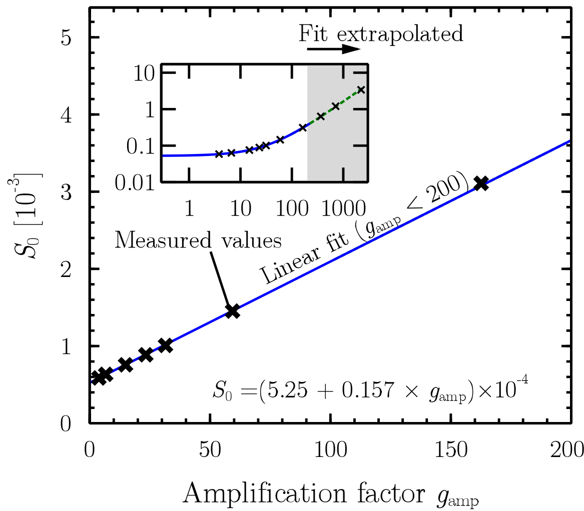

FIG. 6. Dependence of the baseline signal S_0 on the amplification factor g_{amp}. The fit was calculated for $g_{amp} < 200$, which is the typical range for our measurements.

of this correction are covered by the baseline and nonlinearity uncertainty described in Section IV.

IV. UNCERTAINTY ANALYSIS

This section describes the uncertainty contributions by the instrument which we find to be relevant. We outline our procedures for the quantification of these contributions and combine them into a total uncertainty budget for the device. Note that we do not take sample related uncertainty contributions into account because these contributions depend on the specific measurement task and their determination is beyond the scope of this paper. Section V presents an example evaluation of reflectance and transmittance measurements on a silicon wafer, which also includes sample-specific uncertainty contributions. Also note that some of the uncertainty contributions listed in this section cannot be determined rigorously since the device provides only limited access to the detectors and the control parameters for the measurement. Nevertheless, we show how reasonable estimates for these uncertainty contributions can be determined.

A. Repeatability (u_{rpt})

The repeatability describes the statistical variations when a measurement is repeated several times. This uncertainty contribution arises, for instance, from thermal noise of the detector and is not corrected by the monitor measurement. We determine this uncertainty contribution by repeating each measurement 25 times using the cycle-function of the operating software. The arithmetic mean of the results x_i is used as the mean input quantity $\overline{x_i}$. Assuming a normal distribution of the x_i, the uncertainty $u(\overline{x_i}) = u_{rpt}$ is given by

$$u_{rpt}^2 = \frac{\sigma^2}{\sqrt{N-1}}, \tag{13}$$

according to Eq. (4). In the latter equation, σ^2 denotes the variance and N the number of repetitions. The number of 25 repetitions is a trade-off between the measurement time and a sufficiently close approximation of the normal distribution, which is necessary to use the above formula. In principle, a limited number of repeated measurements are described by the Student's t-distribution rather than the normal distribution.[9] However, the t-distribution approaches the normal distribution for a large number of repetitions. For 25 repetitions, the deviation is already of the order of 5% rel.

B. Baseline offset (u_{bl})

Measurements of transmittance use the simplified process Equation (8) without the determination of the 0% baseline. This is possible since the dark signal of the detectors is internally determined and corrected (see Eq. (9)). However, the application of Eq. (8) requires that there is no offset in the 0% baseline signal, as is the case, e.g., for reflectance measurements, where light is scattered at the exit port of the integrating sphere. Such an offset is not taken into account by the internal dark signal correction. In order to verify that there is no offset in the 0% baseline signal, i.e., $S_0 = 0$, the instrument is set up for transmittance measurements and a beam trap is placed at the sample port. Figure 7 shows data resulting from measurements with this configuration.

The top graph contains data curves recorded with the PM detector between 800 nm and 1000 nm; the bottom graph contains data recorded with the PbS detector between 950 nm and 1400 nm. For the latter, the signal correction described in Section III B is applied. The right hand sides show histograms of the data. The PM data show deviations from zero, which do not seem to be caused by noise. However, the deviations are small: 95% of the data points are located in the interval $\pm 2 \times 10^{-5}$. Moreover, no trend pointing towards a systematic deviation is visible. Hence, we assume the baseline offset to be zero and take the deviations into account by a rectangularly distributed uncertainty component u_{bl} of width 2×10^{-5}. For the PbS detector, the situation is different. The measurement

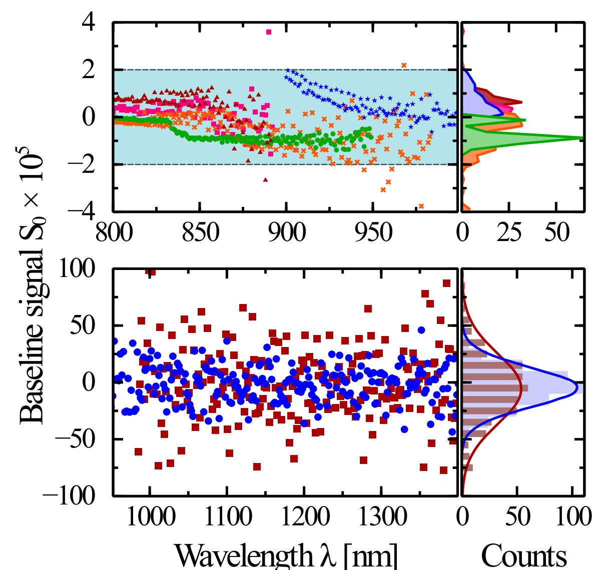

FIG. 7. Measurements of the 0% baseline for transmittance measurements. Each color represents one measurement. Top graph: PM detector; bottom graph: PbS detector; right hand side: Histograms of data.

data exhibit a standard deviation which is up to 50 times higher than their mean. With respect to this scattering, no significant deviation of the mean value from zero is visible. The uncertainty of a PbS measurement result due to random noise will therefore be significantly higher than due to a possible baseline offset. As the random noise is already taken into account in u_{rpt}, we do not have to consider it again here. Hence, the resulting baseline uncertainty is

$$u_{\mathrm{bl}}^2 = \begin{cases} (2 \cdot 10^{-5})^2/3 & \text{PM detector,} \\ 0 & \text{PbS detector.} \end{cases} \quad (14)$$

Note that a potential residual uncertainty of the signal correction outlined in Section III B is covered by u_{bl}^2 when determined experimentally in this way.

C. Nonlinearity of the detectors (u_{nl})

The analysis using the process Equations (7) and (8) assumes a linear relation between the detector signal and the light level in the integrating sphere. Real detector response curves may deviate from the ideal linear relation.[10] This means light with half the intensity of the reference can result in a detector signal higher or lower than 50% of the reference signal. A very sensitive method for determining the nonlinearity of a detector is the *superposition method*,[10] e.g., using two stable light sources. However, this method cannot be applied for the Cary, as the instrument is not prepared for such measurements and the detectors cannot be illuminated externally. Alternatively, nonlinearities could be determined by transmittance measurements on calibrated filters with known attenuation. However, such measurements may be subject to internal reflections in the filters, which may lead to systematic deviations of unknown extent that would be interpreted as nonlinearities. Therefore, our approach is to use apertures with a large number of small pinholes fabricated from 50 μm thick aluminum foils. These apertures serve as neutral density filters, which do not have the problem of possible internal reflections. The calibration of such apertures with respect to transmittance is challenging, since the measured transmittance may depend on the angle of acceptance of the detection system and may therefore be different for different systems. Using absolute values of the transmittance for the determination of nonlinearities may thus be problematic. However, in Ref. 11, it is shown that different nonlinearity characteristics are expected even for different photodetectors of the same type. In order to examine the nonlinearity of the detectors, we thus measure the aperture transmittance with both the PM and the PbS detector at 850 nm and 1100 nm, respectively, and assume that deviations between the results of the two measurements are due to detector nonlinearities. Before, it was experimentally verified that the apparent transmittance is independent of the wavelength. In doing so, we obtain an estimation for the upper limit of possible detector nonlinearities. In order to optimize the precision of this procedure, each measurement is averaged over 30 s in order to reduce the measurement noise. Figure 8 shows the results of our analysis. The data points represent the ratio of the PbS and PM data; the error bars represent the uncertainty of the ratio due to the measurement noise. For small signals, i.e., low transmittance of the aperture,

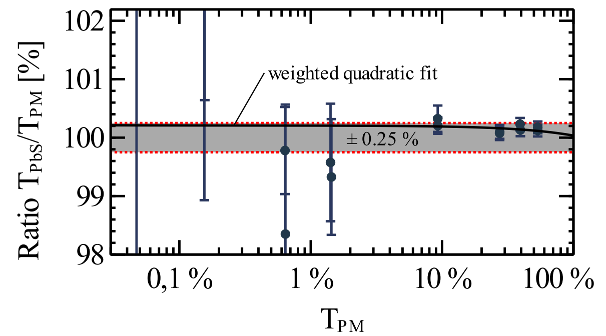

FIG. 8. Ratio of the aperture transmittances measured with the PM and the PbS detector. The solid line represents a weighted quadratic fit of the data.

the uncertainty of the ratio due to the measurement noise is large and the large nonlinearities found here are questionable. We therefore assume that a possible nonlinearity should vary smoothly with the light level and fit the data with a second order polynomial, taking the uncertainty of the data into account as fit weights. The resulting fit curve is represented by the solid line in Fig. 8. Our procedure does not indicate which of the two detectors behaves nonlinear, and the results do not show a clear trend towards over- or underestimation of the signal. From the fit curve, we thus obtain a rectangularly distributed uncertainty component u_{nl} with a width of 0.25% of the measured signal S,

$$u_{\mathrm{nl}}^2 = \frac{(0.25\% \cdot S)^2}{3} . \quad (15)$$

D. Spectral bandwidth of the monochromator (u_{sbw})

For the evaluation of spectrophotometric measurements, illumination with monochromatic light is assumed. In reality, however, the monochromator provides light with a finite bandwidth $\Delta\lambda$. At a nominal wavelength λ_0, this leads to additional signal contributions by radiation incident at neighboring wavelengths. In principle, these additional signal contributions are taken into account by the calibration of the instrument (baseline measurements) because they occur during both the baseline and the sample measurements. However, deviations may occur in regions where the shapes of the baseline and measurement curves are different. In order to correctly resolve narrow features of a spectrum, it may thus be required to use a high spectral resolution (i.e., a small spectral bandwidth) and to apply a spectral deconvolution correction.[12,13] However, if the spectra under investigation do not contain narrow features such as peaks, as is typically the case for our measurements, the spectral bandwidth causes only a small signal contribution compared to the overall uncertainty of the measurement. In this case, a correction can be neglected, and spectral bandwidth effects can be included in the uncertainty budget.[8]

Generally, the detector signal S at the nominal wavelength λ_0 is given by the integral of the product of the spectral irradiance $I(\lambda)$, the bandpass function $B(\lambda)$, and the spectral sensitivity $\eta(\lambda)$ of the monochromator/detector system, multiplied with a scaling factor C which depends on the detector and the read-out electronics,

$$S(\lambda_0) = C \int_0^\infty I(\lambda)\, B(\lambda)\, \eta(\lambda)\, d\lambda\,. \tag{16}$$

In order to estimate the impact of the finite spectral bandwidth on measurements, a rectangular bandpass function of the monochromator

$$B(\lambda) = \begin{cases} \dfrac{1}{\Delta\lambda}, & \lambda_0 - \Delta\lambda/2 \le \lambda \le \lambda_0 + \Delta\lambda/2 \\ 0 & \text{elsewhere} \end{cases} \tag{17}$$

is considered, and a constant spectral sensitivity η of the detector within this wavelength range is assumed. Note that the bandpass function of real monochromators is rather triangular or Gaussian, so that the following considerations may be regarded as a worst case estimation. With these assumptions,

$$S(\lambda_0) = C' \int_{\lambda_0-\Delta\lambda/2}^{\lambda_0+\Delta\lambda/2} I(\lambda)\mathrm{d}\lambda \tag{18}$$

follows. In the latter equation, $C' = C\,\eta/\Delta\lambda$. Using $S(\lambda) = C'\,I(\lambda)$, a second order Taylor approximation for I and the approximation of the second derivative for discrete values leads to the expression[14]

$$u_{\mathrm{sbw}}^2 = \frac{(S_- - 2S_0 + S_+)^2}{108}\,, \tag{19}$$

with $S_- = S(\lambda_0 - \Delta\lambda/2)$ and $S_+ = S(\lambda_0 + \Delta\lambda/2)$. The exemplary uncertainty budget given in Section V shows that u_{sbw} is small compared to the overall uncertainty and thereby verifies our treatment of spectral bandwidth effects. Note that in general, a smaller spectral bandwidth leads to a smaller uncertainty contribution u_{sbw} but also decreases the signal-to-noise ratio, which in turn increases the uncertainty contribution u_{rpt}. For our measurements, a good trade-off is found to be $\Delta\lambda = 8$ nm.

E. Wavelength calibration of the instrument (u_{wc})

Wavelength deviations lead to a wrong assignment of measurand (R or T) and wavelength and can thus be interpreted as artificial signal contributions with a positive or negative sign, depending on the shape of the spectrum and the direction of the deviation. In order to prevent such deviations, the monochromator is automatically calibrated with respect to the wavelength using a Hg source when the device is started. The accuracy and precision of the grating monochromator are tested and recorded during the yearly maintenance. For our device, the accuracy is found to be ±0.05 nm at maximum for all wavelengths without systematic deviations. Moreover, the repeatability of the wavelength adjustment is found to be ≤0.003 nm. The latter value characterizes the maximum deviation between the baseline and sample measurements, from which R or T are calculated. Since it is more than one order of magnitude below the uncertainty of the absolute wavelength adjustment, the uncertainty contribution due to the wavelength adjustment is estimated for the final data (R or T) only, and the single baseline and sample measurements are assumed to be free of wavelength deviations. We estimate an upper limit of the uncertainty of R or T at the nominal wavelength λ_0 by interpolating the data between $\lambda_0 \pm \delta\lambda$ and using the maximum difference to the data at λ_0. This deviation is taken into account as a rectangularly distributed uncertainty contribution

$$u_{\mathrm{WC}}^2(\lambda_0) = \frac{\max\left(M(\lambda_0) - M(\lambda_0 \pm \delta\lambda)\right)^2}{3}, \tag{20}$$

with $M \in \{R, T\}$. Note that we do not observe a systematic wavelength deviation after the calibration of the instrument and thus do not need to apply a correction. Additionally note that estimating this uncertainty component for the resulting reflectance or transmittance curve rather than for the single baseline and sample measurements would not be possible if the reproducibility was of the same order of magnitude as the wavelength accuracy. In this case, the wavelength uncertainty must be considered for each measurement, and a different sensitivity coefficient has to be used in Eqs. (24) and (31).

F. Uncertainty caused by the reflectance standard (u_{std})

For reflectance measurements, a primary calibrated standard is used. Its uncertainty u_{std} is taken from the calibration certificate and interpolated linearly for the specific wavelength. Note that calibration certificates usually contain the uncertainty for a coverage factor $k = 2$, from which the standard uncertainty required for the uncertainty budget is obtained by dividing by 2.

G. Reproducibility (u_{rpd})

Fluctuations and drifts of the detector signal may occur on timescales of days or months. This may be due to slowly changing parameters like humidity or ambient temperature, which might affect the adjustment of the optical components of the instrument. Moreover, the positioning of the sample and other operator-related parameters may affect the reproducibility of spectrophotometric measurements as well. This uncertainty contribution is experimentally determined by repeating a reflectance measurement of a polished silicon wafer in the wavelength range from 250 nm to 2000 nm over the course of several months. The maximum deviation of the results is found to be 0.25% rel. for all wavelengths and a systematic wavelength dependence is not observed. Thus, we take the reproducibility into account by a rectangularly distributed uncertainty component

$$u_{\mathrm{rpd}}^2 = \frac{(0.25\% \cdot S)^2}{3}, \tag{21}$$

where S is the measurand (R or T). Note that we do not consider this contribution for the single baseline and sample measurements.

H. Calculation of the uncertainty budget

The uncertainty budget is calculated according to Eqs. (3), (7), and (8), respectively.

(1) Transmittance measurements:

First, the uncertainties of T_{N} and T_{S} need to be calculated, which are

$$u_{T_{\mathrm{S}}}^2 = u_{\mathrm{sbw}}^2 + u_{\mathrm{rpt}}^2, \tag{22}$$

$$u_{T_{\mathrm{N}}}^2 = u_{\mathrm{sbw}}^2 + u_{\mathrm{rpt}}^2. \tag{23}$$

TABLE I. Uncertainty contributions due to properties of our instrument for measurements of transmittance (T) and reflectance (R).

T/R	Description	Symbol	Our value	Distribution	Sens. coeff.
R	Refl. standard	u_{std}	(2.981 to 3.664) $\times 10^{-3}$[a]	Normal	— / $c_{R_{\mathrm{Std}}}$
T/R	Nonlinearity	u_{nl}	$1.443 \times 10^{-3} S$[a]	Rectangular	1 / 1
T/R	Reproducibility	u_{rpd}	$1.443 \times 10^{-3} S$[a]	Rectangular	1 / 1
T/R	Repeatability	$u_{\mathrm{rpt,S}}$	Eq. (13)[a]	Normal	$c_{T_{\mathrm{S}}}$ / $c_{R_{\mathrm{S}}}$
R	Repeatability	$u_{\mathrm{rpt,B}}$	Eq. (13)[a]	Normal	— / $c_{R_{\mathrm{B}}}$
T/R	Repeatability	$u_{\mathrm{rpt,N}}$	Eq. (13)[a]	Normal	$c_{T_{\mathrm{N}}}$ / $c_{R_{\mathrm{N}}}$
T/R	Spectr. bandwidth	$u_{\mathrm{sbw,S}}$	$\Delta\lambda = 8$ nm, Eq. (19)[a]	Rectangular	$c_{T_{\mathrm{S}}}$ / $c_{R_{\mathrm{S}}}$
T/R	Wavelength cal.	u_{wc}	$\delta\lambda = 0.05$ nm, Eq. (20)[a]	Rectangular	1 / 1
T/R	Spectr. bandwidth	$u_{\mathrm{sbw,N}}$	$\Delta\lambda = 8$ nm, Eq. (19)[a]	Rectangular	$c_{T_{\mathrm{N}}}$ / $c_{R_{\mathrm{N}}}$
T	Baseline	u_{bl}	1.155×10^{-5}	rectangular	1 /—

[a]To be calculated for each wavelength.

With this and Eq. (8), the uncertainty of T follows as

$$u_T^2 = c_{T_{\mathrm{S}}}^2 \cdot u_{T_{\mathrm{S}}}^2 + c_{T_{\mathrm{N}}}^2 \cdot u_{T_{\mathrm{N}}}^2 + u_{\mathrm{rpd}}^2 + u_{\mathrm{nl}}^2 + u_{\mathrm{wc}}^2 + u_{\mathrm{bl}}^2, \quad (24)$$

with the sensitivity coefficients

$$c_{T_{\mathrm{S}}}^2 = \frac{1}{{T_{\mathrm{N}}}^2}, \quad (25)$$

$$c_{T_{\mathrm{N}}}^2 = \frac{{T_{\mathrm{S}}}^2}{{T_{\mathrm{N}}}^4}. \quad (26)$$

(2) Reflectance measurements:

The uncertainties of the input quantities are

$$u_{R_{\mathrm{S}}}^2 = u_{\mathrm{sbw}}^2 + u_{\mathrm{rpt}}^2, \quad (27)$$

$$u_{R_{\mathrm{N}}}^2 = u_{\mathrm{sbw}}^2 + u_{\mathrm{rpt}}^2, \quad (28)$$

$$u_{R_{\mathrm{B}}}^2 = u_{\mathrm{rpt}}^2, \quad (29)$$

$$u_{R_{\mathrm{Std}}}^2 = u_{\mathrm{std}}^2. \quad (30)$$

With Eq. (7), the uncertainty of R is then

$$u_R^2 = c_{R_{\mathrm{S}}}^2 \cdot u_{R_{\mathrm{S}}}^2 + c_{R_{\mathrm{N}}}^2 \cdot u_{R_{\mathrm{N}}}^2 + c_{R_{\mathrm{B}}}^2 \cdot u_{R_{\mathrm{B}}}^2 + + c_{R_{\mathrm{Std}}}^2 \cdot u_{R_{\mathrm{Std}}}^2 + u_{\mathrm{rpd}}^2 + u_{\mathrm{nl}}^2 + u_{\mathrm{wc}}^2, \quad (31)$$

with the sensitivity coefficients

$$c_{R_{\mathrm{S}}}^2 = \left(\frac{1}{R_{\mathrm{N}} - R_{\mathrm{B}}} R_{\mathrm{Std}}\right)^2, \quad (32)$$

$$c_{R_{\mathrm{N}}}^2 = \left(\frac{R_{\mathrm{S}} - R_{\mathrm{B}}}{(R_{\mathrm{N}} - R_{\mathrm{B}})^2} R_{\mathrm{Std}}\right)^2, \quad (33)$$

$$c_{R_{\mathrm{B}}}^2 = \left(\frac{R_{\mathrm{S}} - R_{\mathrm{N}}}{(R_{\mathrm{N}} - R_{\mathrm{B}})^2} R_{\mathrm{Std}}\right)^2, \quad (34)$$

$$c_{R_{\mathrm{Std}}}^2 = \left(\frac{R_{\mathrm{S}} - R_{\mathrm{B}}}{R_{\mathrm{N}} - R_{\mathrm{B}}}\right)^2. \quad (35)$$

Table I summarizes the uncertainty contributions as determined in this work. Uncertainties related to the specific properties of the sample add to the total uncertainty and need to be considered as well for a complete analysis of a specific measurement.

V. EXAMPLE UNCERTAINTY ANALYSIS

Figure 9 shows measurements of the reflectance and transmittance of a planar cz-silicon wafer with polished surfaces, which were carried out for the determination of the absorption coefficient of crystalline silicon.[15,16] For these measurements, an additional uncertainty contribution for the sample's geometry is taken into account. This contribution takes internal reflections of light in the sample and the partial polarization of the incident light into account. It is estimated using the literature data of the index of refraction,[17] the angle of incidence of the light beam, as well as the experimentally determined degree of polarization. Snell's law is then used to calculate the maximum deviation, which is taken into account as a rectangularly distributed uncertainty component u_{sg} and added to u_{T} and u_{R}.

The determined uncertainty ($k = 2$) is around 1% relative for reflectance measurements. For measurements of transmittance, the uncertainty is 0.4% relative in the wavelength range where $T > 0.25$. Figure 10 visualizes the uncertainty budget at 970 nm and 1135 nm. The bars represent the summands of Eqs. (24) and (31). The accuracy of the reflectance measurement is limited by the uncertainty u_{std} of the reflectance standard for all wavelengths. Hence, the instrument does not add significant uncertainty to the measurement data, and its accuracy is obviously sufficient for this purpose. The uncertainty of the transmittance measurement is dominated by the reproducibility (u_{rpd}) and nonlinearity (u_{nl}) if $T > 0.15$. For 0.15 $> T > 0.0002$, the noise of the sample measurement ($u_{\mathrm{rpt,S}}$) dominates the overall uncertainty. For smaller transmission,

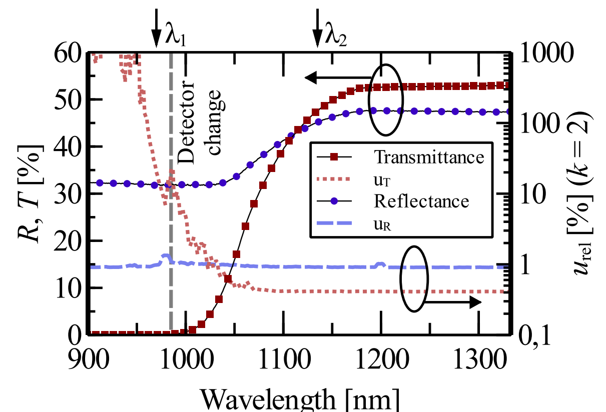

FIG. 9. Exemplary measurement of a polished silicon wafer. The detectors are changed at 985 nm. For the wavelengths $\lambda_{1/2}$, the corresponding uncertainty budget is given in Fig. 10.

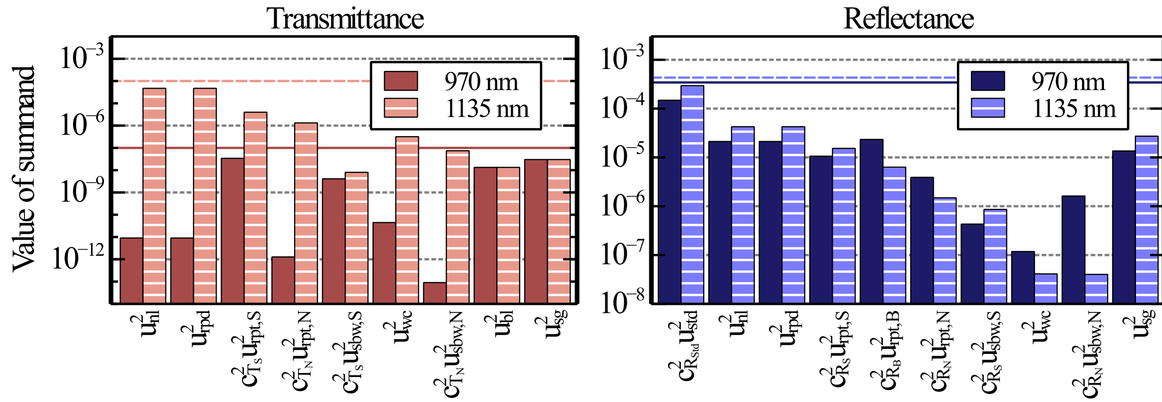

FIG. 10. Visualization of the uncertainty budget of the data shown in Fig. 9 for 970 nm and 1135 nm. The bars represent the summands of Eqs. (24) and (31). The lines visualize the sums of the corresponding contributions.

the sample geometry (u_{sg}) and baseline uncertainty (u_{bl}) contributions become dominant.

VI. CONCLUSIONS

We conduct an analysis of the instrument-related uncertainty of measurements of reflectance and transmittance with the commercially available Agilent Cary 5000 spectrophotometer. The analysis is based on an extensive characterization of the instrument and the specifications of the *Guide to the expression of uncertainty in measurements* (GUM). We present methods for the experimental determination of the uncertainty contributions and combine them into an uncertainty budget. Our analysis takes uncertainties due to repeatability, reproducibility, baseline offsets, detector nonlinearity, spectral bandwidth, wavelength calibration of the instrument, and uncertainty of the reflectance standard into account. The methods and procedures outlined in this paper are applicable to any spectrophotometer. Moreover, we optimize the measurement procedure and the device settings in order to improve the signal-to-noise ratio of the data, which reduces the overall uncertainty. Systematic measurement deviations are identified and corrected. We thereby increase the usable dynamic range of our instrument by one order of magnitude.

ACKNOWLEDGMENTS

The authors would like to thank Dr. E. Daub from Siltronic for his support and for providing polished silicon wafers. Many thanks also goes to C. Marquardt (ISFH) for processing the samples and to R. Reinecke-Koch (ISFH) for fruitful discussions about the instrumentation and the uncertainty analysis, which provided valuable input for this paper. We thank the anonymous reviewers for their help in improving this paper.

APPENDIX: DERIVATION OF THE SIGNAL CORRECTION FOR THE PBS DETECTOR

In order to obtain a correction that determines the corrected signal S from the signal levels S'_{Sam}, S'_{Mon}, and S'_{Bas} which are actually measured due to the inertia of the detector and/or measurement amplifier and give

$$S' = \frac{S'_{\text{Sam}} - S'_{\text{Bas}}}{S'_{\text{Mon}} - S'_{\text{Bas}}}, \tag{A1}$$

instead of S (see Eq. (9)), a model of the detector signal as a function of time is required. Depending on the physical origin of the inertia effect, different functions can be assumed. It should be noted that the exact procedure for the determination of the detector signal is unknown. However, as shown below, the different corrections obtained by assuming different functions lead to the same results within ±0.01% absolute.

Case 1: Exponential decay

A decay of the charge carrier concentration within the detector is one possible reason for the occurrence of the inertia effect. In this case, the signal would be expected to decay exponentially. The time-dependent detector output signal $S'(t)$ is then given by

$$S'(t) = \begin{cases} S_{\text{Mon}} + \left(S'(0) - S_{\text{Mon}}\right) e^{-\beta t}, & 0 \le t \le \tau \\ S_{\text{Sam}} + \left(S'(\tau) - S_{\text{Sam}}\right) e^{-\beta(t-\tau)}, & \tau \le t \le 2\tau \\ S_{\text{Bas}} + \left(S'(2\tau) - S_{\text{Bas}}\right) e^{-\beta(t-2\tau)}, & 2\tau \le t \le 3\tau \end{cases} \tag{A2}$$

and

$$S'(t) = S'(t + n \times 3\tau), \; n = 0, 1, 2, \ldots. \tag{A3}$$

In these equations, β is the (unknown) time constant of the signal decay and τ the duration of the illumination of each channel. S_{Mon}, S_{Sam}, and S_{Bas} denote the saturation levels of the signal as defined in Fig. 5. The general solution to Eqs. (A2) and (A3) is

$$S'(t) = \begin{cases} S_{\text{Mon}} + c_{\text{Mon}} \mathrm{e}^{-\beta t}, & 0 \le t \le \tau \\ S_{\text{Sam}} + c_{\text{Sam}} \mathrm{e}^{-\beta(t-\tau)}, & \tau \le t \le 2\tau, \\ S_{\text{Bas}} + c_{\text{Bas}} \mathrm{e}^{-\beta(t-2\tau)}, & 2 \le t \le 3\tau \end{cases} \tag{A4}$$

with

$$c_{\rm Mon} = \frac{S_{\rm Sam} - S_{\rm Mon} + (S_{\rm Bas} - S_{\rm Mon})e^{-\beta\tau}}{1 + e^{-\beta\tau} + e^{-2\beta\tau}}, \quad (A5)$$

$$c_{\rm Sam} = \frac{S_{\rm Bas} - S_{\rm Sam} + (S_{\rm Mon} - S_{\rm Sam})e^{-\beta\tau}}{1 + e^{-\beta\tau} + e^{-2\beta\tau}}, \quad (A6)$$

$$c_{\rm Bas} = \frac{S_{\rm Mon} - S_{\rm Bas} + (S_{\rm Sam} - S_{\rm Bas})e^{-\beta\tau}}{1 + e^{-\beta\tau} + e^{-2\beta\tau}}. \quad (A7)$$

A reasonable assumption would be that the detector signal is integrated over a period of time in order to reduce the measurement noise. In general, the signal is integrated from t_1 to t_2, where

$$n\,\tau \le t_1 \le t_2 \le (n+1)\,\tau\,,\ n = 0,1,2\,. \quad (A8)$$

This leads to

$$S'_{\rm Mon} = \int_{t_1}^{t_2} S'(t)\,dt\,, \quad (A9)$$

$$S'_{\rm Sam} = \int_{\tau+t_1}^{\tau+t_2} S'(t)\,dt\,, \quad (A10)$$

$$S'_{\rm Bas} = \int_{2\tau+t_1}^{2\tau+t_2} S'(t)\,dt\,. \quad (A11)$$

Combining Eqs. (A2)–(A8) leads to

$$S'_{\rm Mon} = S_{\rm Mon}(t_2 - t_1)\tau + \frac{c_{\rm Mon}}{\beta}\left(e^{-\beta\tau t_1} - e^{-\beta\tau t_2}\right), \quad (A12)$$

$$S'_{\rm Sam} = S_{\rm Sam}(t_2 - t_1)\tau + \frac{c_{\rm Sam}}{\beta}\left(e^{-\beta\tau t_1} - e^{-\beta\tau t_2}\right), \quad (A13)$$

$$S'_{\rm Bas} = S_{\rm Bas}(t_2 - t_1)\tau + \frac{c_{\rm Bas}}{\beta}\left(e^{-\beta\tau t_1} - e^{-\beta\tau t_2}\right). \quad (A14)$$

The case of signal sampling at distinct times $t_{\rm Mon}$, $t_{\rm Sam}$, and $t_{\rm Bas}$, which is considered in Fig. 5 for the purpose of simplicity, is contained in these equations as the special case $t_2 \to t_1$. Note that for an instant change of the signal level, i.e., $\beta \to \infty$, the second terms on the right hand sides disappear and the terms $(t_2 - t_1)\tau$ cancel out when inserting the results into Eq. (A2) or (9), respectively, which is the correct result for this case, where a correction is not required. Inserting Eqs. (A12)–(A14) into Eq. (A1) leads to

$$S' = \frac{S_{\rm Sam} - S_{\rm Bas} + K\,(c_{\rm Sam} - c_{\rm Bas})}{S_{\rm Mon} - S_{\rm Bas} + K\,(c_{\rm Mon} - c_{\rm Bas})}, \quad (A15)$$

with

$$K = \frac{e^{-\beta t_1\tau} - e^{-\beta t_2\tau}}{\beta(t_2 - t_1)\tau}. \quad (A16)$$

The equation can further be simplified by recognizing that the constant signal offset described by the baseline signal $S_{\rm Bas}$ is also contained in $S_{\rm Mon}$ and $S_{\rm Sam}$. As Eq. (A15) only contains signal differences, any constant offset cancels out and $S_{\rm Bas} = 0$ can be assumed without loss of generality. Moreover, the two-channel measurement technique only considers the ratio of $S_{\rm Sam}$ to $S_{\rm Mon}$ but not the absolute values of these quantities. Therefore, we can scale both $S_{\rm Sam}$ and $S_{\rm Mon}$ with a scaling factor such that $S_{\rm Mon} = 1$ without changing the result of Eq. (A15). Hence, the equation can be simplified further by setting $S_{\rm Mon} = 1$.

With these simplifications, Eq. (A15) contains two unknowns, namely, $S_{\rm Sam}$, which is to be determined, and the factor K which accounts for the integration limits and the time constant β. The quantity S' is known from the measurement. In order to obtain $S_{\rm Sam}$, a measurement of the 0% baseline S_0 using a beam trap is required. For this situation, $S_{\rm Sam} = S_{\rm Bas} = 0$ holds and Eq. (A15) becomes

$$S' = S_0 = \frac{(e^{-\beta\tau} - 1)(e^{-\beta t_1\tau} - e^{-\beta t_2\tau})}{(1 + e^{-\beta\tau} + e^{-2\beta\tau}\beta\tau)(t_2 - t_1) - (e^{-\beta\tau} + 2)(e^{-\beta t_1\tau} - e^{-\beta t_2\tau})}. \quad (A17)$$

Combining Eqs. (A15) and (A17) yields

$$S_{\rm Sam} = \frac{S' - S_0}{1 + S_0\,(S' - 1)}. \quad (A18)$$

Since we assumed $S_{\rm Bas} = 0$ and $S_{\rm Mon} = 1$,

$$S = S_{\rm Sam} \quad (A19)$$

holds according to Eq. (9), which finally leads to

$$S = \frac{S' - S_0}{1 + S_0\,(S' - 1)}, \quad (A20)$$

which is the correction formula Eq. (11).

Case 2: Linear decay

Inertia of the measurement amplifier is another possible reason for the occurrence of the inertia effect. In this case, a linear signal decay with constant slope would be expected. The dependence of the measured 0% baseline signal on the amplification factor points towards the measurement amplifier as the origin of the effect. Assuming that the detector signal is given by the integral over the period τ, the signal levels $S'_{\rm Mon}$, $S'_{\rm Sam}$, and $S'_{\rm Bas}$ follow as

$$S'_{\rm Mon} = S_{\rm Mon}\,\tau + (S_{\rm Bas} - S_{\rm Mon})\,\frac{\Delta t_1}{2}, \quad (A21)$$

$$S'_{\rm Sam} = S_{\rm Sam}\,\tau + (S_{\rm Mon} - S_{\rm Sam})\,\frac{\Delta t_2}{2}, \quad (A22)$$

$$S'_{\rm Bas} = S_{\rm Bas}\,\tau + (S_{\rm Sam} - S_{\rm Bas})\,\frac{\Delta t_3}{2}. \quad (A23)$$

Since the signal decay is linear with constant slope a,

$$\Delta y = a\,\Delta t \quad (A24)$$

holds where Δy denotes the amplitude of the signal change. Combining the latter equations yields

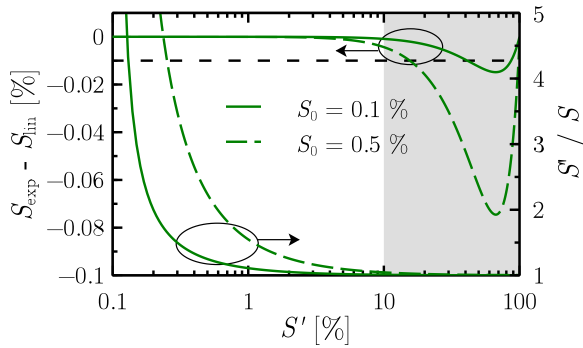

FIG. 11. Comparison of the correction formulas for exponential and linear decay, expressed as the absolute difference between both corrections as a function of the uncorrected signal S'. On the right axis, the significance of the correction is shown.

$$S'_{\mathrm{Mon}} = S_{\mathrm{Mon}}\,\tau - \frac{(S_{\mathrm{Bas}} - S_{\mathrm{Mon}})^2}{2a}, \tag{A25}$$

$$S'_{\mathrm{Sam}} = S_{\mathrm{Sam}}\,\tau + \frac{(S_{\mathrm{Mon}} - S_{\mathrm{Sam}})^2}{2a}, \tag{A26}$$

$$S'_{\mathrm{Bas}} = S_{\mathrm{Bas}}\,\tau + \frac{(S_{\mathrm{Sam}} - S_{\mathrm{Bas}})^2}{2a}. \tag{A27}$$

Inserting this result into Eq. (A1) and following the derivation outlined above, the correction formula

$$S = \frac{\sqrt{(1-4S')S_0{}^2 + (4S'^2-2)S_0 + 1} + S_0 - 1}{2\,S'\,S_0} \tag{A28}$$

is obtained.

A comparison of the correction formulas Eqs. (A20) and (A28) for exponential or linear decay, respectively, is shown in Fig. 11. Figure 11 shows the absolute deviation between the corrected values using the correction for the exponential or linear decay, respectively, as a function of the measured (uncorrected) signal S'. It can be seen that the absolute deviation between both corrections is below 0.01% for signal levels below 10%, where the correction has a significant impact, i.e., $S'/S > 1$. Compared to the uncertainty of the measured data, this deviation can be neglected, i.e., both corrections yield the same results. For the purpose of simplicity, the correction formula for the exponential decay is thus used in this work.

[1]H.-H. Perkampus, H.-C. Grinter, and T. L. Threlfall, *UV-VIS Spectroscopy and its Applications* (Springer, 1992).
[2]J. Workman, Jr. and A. Springsteen, *Applied Spectroscopy: A Compact Reference for Practitioners* (Academic Press, 1998).
[3]K.-E. Peiponen, R. Myllylä, and A. V. Priezzhev, *Optical Measurement Techniques: Innovations for Industry and the Life Sciencess* (Springer, 2009), Vol. 136.
[4]J. Dobilienė, E. Raudienė, and R. P. Žilinskas, Measurement **43**, 113 (2010).
[5]P. S. Ramanjaneyulu, Y. S. Sayi, and K. L. Ramakumar, Indian J. Chem. Technol. **17**, 468 (2010), available at http://nopr.niscair.res.in/handle/123456789/10721?mode=full.
[6]ASTM International, Standard Practice for Estimating Uncertainty of Test Results Derived from Spectrophotometry, 10.1520/E2867-13, 2013.
[7]L. Sooväli, E.-I. Rõõm, A. Kütt, I. Kaljurand, and I. Leito, Accredit. Qual. Assur. **11**, 246 (2006).
[8]Joint Committee for Guides in Metrology, JCGM, 100, 2008.
[9]B. J. Winer, D. R. Brown, and K. M. Michels, *Statistical Principles in Experimental Design* Vol. 2 (McGraw-Hill, New York, 1971).
[10]S. Yang, I. Vayshenker, X. Li, and T. R. Scott, "Accurate measurement of optical detector nonlinearity," Technical Report (National Institute of Standards and Technology, 1994).
[11]W. Budde, Appl. Opt. **18**, 1555 (1979).
[12]E. R. Woolliams, R. Baribeau, A. Bialek, and M. G. Cox, Metrologica **48**, 164 (2011).
[13]S. Eichstädt, F. Schmähling, G. Wübbeler, K. Anhalt, L. Bünger, U. Krüger, and C. Elster, Metrologica **50**, 107 (2013).
[14]I. Bronstein and K. Semendjaev, *Taschenbuch der Mathematik* (Verlag Harri Deutsch, 2001).
[15]C. Schinke, K. Bothe, P. C. Peest, J. Schmidt, and R. Brendel, Appl. Phys. Lett. **104**, 081915 (2014).
[16]C. Schinke, P. C. Peest, J. Schmidt, R. Brendel, K. Bothe, M. R. Vogt, I. Kröger, S. Winter, A. Schirmacher, S. Lim, H. Nguyen, and D. MacDonald, AIP Adv. **5**, 067168 (2015).
[17]M. A. Green, Sol. Energy Mater. Sol. Cells **92**, 1305 (2008).